


Article

Spray Printing of Porous Substrates from Nanosuspensions

David H. Panduro Vela ¹, Carola Schlumberger ², Matthias Thommes ² and Andreas Bück ^{1,*} 

¹ Institute of Particle Technology, Friedrich-Alexander-Universität Erlangen-Nürnberg, Cauerstr. 4, D-91058 Erlangen, Germany

² Institute of Separation Science and Technology, Friedrich-Alexander-Universität Erlangen-Nürnberg, Egerlandstr. 3, D-91058 Erlangen, Germany

* Correspondence: andreas.bueck@fau.de

Abstract: In this work, we present and characterise an experimental setup that allows the generation of porous packings from nanosuspensions. By defined positioning and drying of solid-containing droplets, large-scale porous structures can be generated. Examples of such structures are shown and characterised. Operational challenges are presented, and it is discussed how they can be overcome to allow the maximum degree of freedom in packing generation.

Keywords: drying; drop-on-demand; suspension; porosity; textural characterization

1. Introduction

Chromatography, the fractionation of (molecular) components according to their intrinsic properties, depends on the defined interaction of the components with a stationary phase material (SPM) while being transported in a carrier fluid through the pore space of that SPM. The efficiency and selectivity of fractionation is therefore the outcome of a complex multi-scale, multiphase process.

A main problem observed in the realization and operation of chromatography and packed bed processes in general is that the transport of carrier fluid and components, and heat and mass transfer depend on the structure of the packing, i.e., the spatial arrangement of the SPM in the apparatus and the properties of the generated pore space. The pore space is characterized by a complex pore network, determining, e.g., the porosity (radially, axially), the pore size distribution, the connectivity of pores, as well as the tortuosity of paths through the SPM. The extent of spatial distribution, e.g., in porosity, and property distributions, such as pore size, has a significant influence on the efficiency, capacity and selectivity of an SPM in a chromatographic separation task.

Synthesized (spherical) chromatographic beads, e.g., from spray-drying [1], are typically assembled into packings by filling the material into the chromatographic column followed by a compaction process, e.g., application of an external pressure. It is well-known that in packed beds the porosity in radial direction increases towards the apparatus walls, creating a centre zone that is less porous than the outer zone. Classical works, e.g., by Martin [2], have shown that even small high-porosity zones may have huge influences on flow distribution (residence time distribution of fluid, resp.), heat and mass transfer, and on the performance indicators. Well defined stationary phase packings are therefore a major handle towards efficient and selective separation in chromatography.

As a consequence, the design of a new functional SPM must be accompanied by the development of techniques for defined and optimized packing structures to minimize flow maldistribution and broadening of residence time distributions and maximize the selective interaction of the components with functionalised SPM.

In the broader context of fixed beds with defined packing structures and applications in catalysis and liquid chromatography, two main approaches are currently investigated: self-assembly of colloidal particles into (dense) structures, e.g., pillar arrays [3], monoliths [4],



Citation: Panduro Vela, D.H.; Schlumberger, C.; Thommes, M.; Bück, A. Spray Printing of Porous Substrates from Nanosuspensions. *Processes* **2023**, *11*, 1143. <https://doi.org/10.3390/pr11041143>

Academic Editor: Ofélia Anjos

Received: 22 February 2023

Revised: 4 April 2023

Accepted: 5 April 2023

Published: 7 April 2023



Copyright: © 2023 by the authors. Licensee MDPI, Basel, Switzerland. This article is an open access article distributed under the terms and conditions of the Creative Commons Attribution (CC BY) license (<https://creativecommons.org/licenses/by/4.0/>).

or vacuum-assisted layer-wise methods [5,6]. The practicality of these approaches are currently limited by either producing too dense packings or in challenges going from single- to multi-layer specimens.

The second main approach is the use of various additive manufacturing techniques. Periodic porous structures have been generated in metal-based processes, e.g., cellular structures with pore sizes typically larger than 100 μm by selective electron beam melting [7–9], achieving significant increases in heat and mass transfer in liquid chromatography. Using polymers as base materials with particulate additives, e.g., metals or ceramics, very defined structures at a (sub-)micrometer scale have been achieved [10–12]. The techniques with the highest resolution are currently two photon photopolymerization techniques, with a spatial resolution of down to 30 nm [13]. Variation of the size and shape of the particulates also allows production of homogeneous structures with low porosity, e.g., by temporary use of spacer particles or porogens [14,15].

The major challenge in the use of polymers is that compatible systems need to be found, i.e., photoinitiators, photoabsorbers, materials that cross-link well with the particles and tight reaction control are required. In terms of functionalisation, some of the particles are included in the polymer matrix, i.e., they are not accessible for interaction with the carrier fluid or other particulates, such as NP dispersed in the fluid.

The use of suspensions of functionalized colloidal particles to generate porous packings has not yet attracted comparable attention. The potential here lies in the wide variety of combinations of liquids and solids, as well as in the many different options for functionalisation of the colloidal particles. Moreover, the excessive loss of the functional surface due to incorporation of the active particulates into the volume of a support medium (e.g., polymer) is avoided. A third advantage over other techniques is that the spatial structure of the packing can be manipulated over a wide range, e.g., by using polydisperse particles and the inclusion of spacer particles.

The key working principle is the solids deposit formation from the evaporating sessile droplet. The first investigations were presented in the seminal work by Deegan et al. [16] on the coffee-ring effect that related the pattern formation to differences in the evaporation profile along the liquid–gas interface of the sessile droplet. For an in-depth study of the intradroplet processes, we refer to the review by Larson [17] and the additional experimental investigations and explanations in Sondej et al. [18]. Therein, it is shown that the shape of the deposit can be manipulated by the gas-side drying conditions.

Via the modelling of drying of colloidal suspensions, either free or sessile droplets, e.g., in [19,20], further main influences on structure formation from single droplets were derived, for instance, regarding gas-side conditions or functionalisation of the colloidal particles. Recent works of Janocha and Tsotsas on structure formation during spray coating (i.e., towards layer formation) provide significant insights [21,22]: They showed by small scale experiments (individual droplets, at most three stacked on top of each other) the influence of material and drying conditions on the evaporation profiles. Using tomographic methods, they also provided insight into porosity and internal structure formation of the deposits.

In this work, we report on the development and characterisation of a new scalable technology for the continuous production of stationary phase materials from suspensions by spray printing. The porous substrate is generated by a layer-by-layer build-up from individual droplet placement and convective drying.

The work is structured as follows: In Section 2, we present the new apparatus for the production of the porous substrates and characterisation of the main materials used in the studies and the porous structures. Then, a presentation of exemplary results follows, including a discussion of the major challenges of the manufacturing process and how to overcome them. The contribution closes with conclusions and an outlook on future work.

2. Materials and Methods

In this section, we introduce the spray printing setup. We also describe the fundamentals of sessile droplet drying as the main building block for build-up of large-scale porous structures. Furthermore, the materials (solid, liquid, gas) and experimental conditions are introduced as well as the main characterisation methods.

2.1. Spray Printing Setup

The main working principle of the spray printing setup is drop-on-demand casting. In the context of spray printing, only the required amount of droplets are placed at specified locations—either on a substrate or onto a pre-manufactured porous substrate. The structures are formed from solid-containing (i.e., nanoparticles) liquids; the liquid is evaporated by a heated gas flow, leading to the generation of a solid deposit from each droplet. Rational placement of droplets and control of drying conditions allow construction of porous layers of arbitrary shape and size. Repetition of this process yields a layer-by-layer build up of the porous substrate (Figure 1).



Figure 1. Simplified scheme of porous substrate formation by layer-by-layer build-up from single droplet deposits (repeated execution of steps 1 and 2). The liquid of the droplets is evaporated into a heated gas.

The equipment used in this study is schematically presented in Figure 2 (assembled from components manufactured by DataPhysics Instruments GmbH, Filderstadt, Germany): The main component is an optical bench (OCA 200), typically used for contact angle measurements. The optical bench (platform, 10-by-10 cm²) can be positioned automatically relative to the position of the syringes in the x- and y-directions (left/right; front/back) as well as the z-direction (up/down). The spatial resolution and accuracy of movement are 500 nm (x- and y-direction) and 500 μm (z-direction), respectively. Maximum speeds in the x-, y-, z-direction are 14 mm/s, 16 mm/s and 20 mm/s, respectively. The coarser resolution in the z-direction is due to the necessity to move the complete construction that requires additional mechanical stability to withstand larger external forces.

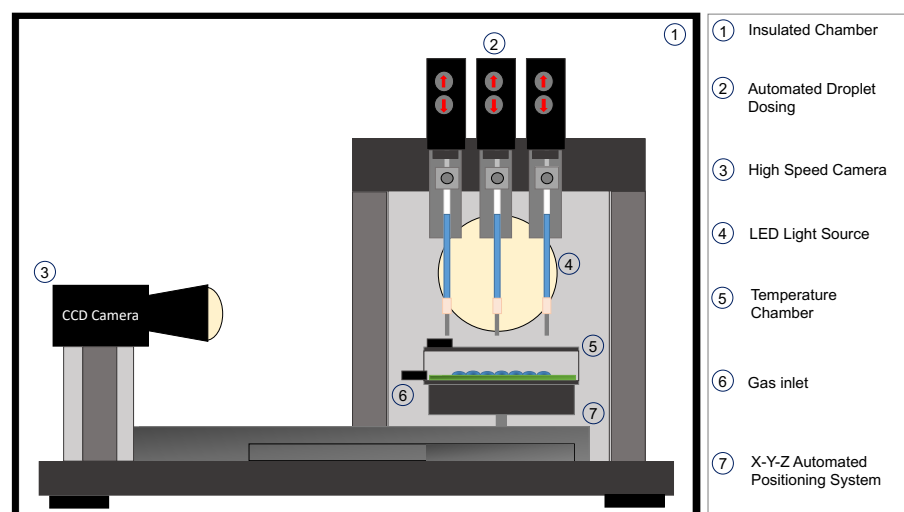


Figure 2. Schematic representation of the main components of the spray printing setup. Not shown: Data acquisition modules.

The optical bench carries a temperature chamber into which the initial substrate is placed on which the porous layers are formed. To this chamber, a gas flow with a defined temperature and initial moisture content is provided. Contact of the gas and the droplets and porous substrates leads to the evaporation of the liquid and deposit formation.

An additional main component is an array of three automated syringes that is positioned on top of the optical bench. Different syringes (dispensing volumes and droplet sizes) can be installed and operated simultaneously. For the purpose of this study, each syringe has a volume of 1 mL and a tip diameter of 0.8 mm. The initial x-, y- and z-position of the syringes was set to 70 mm, 100 mm, and 6 mm, respectively.

The droplet position pattern can be chosen either from a library of patterns or can be designed freely via the automation software of the dispensing system (SCA, DataPhysics Instruments GmbH, Germany).

An LED light source provides sufficient illuminations to generate shadow projections of the placed droplets and porous substrates. Realtime information on the process is obtained by high-speed imaging using a CCD camera coupled with a 7-fold zoom lens with controlled software, motorized focus (± 4.5 mm) and adjustment of the observation angle (approx. 10 degrees). The image size of the camera is a maximal 1544-by-1088 pixels; the maximum sample rate is 78 images per second at this image size.

The whole setup is housed in a container to prevent changing environmental conditions influencing the structure formation. Furthermore, it is decoupled from environmental vibrations.

2.2. Nanosuspension Preparation and Characterisation

The preparation of the nanosuspension is described as well as the characterisation methods for suspension properties important for spray printing.

2.2.1. Suspension Preparation

A technical nanosilica suspension (Köstrosol 4550, CWK-BK GmbH, Bad Köstritz, Germany) with a concentration of 49.5 wt-% and a primary particle size of 45 nm was used throughout the investigations. Suspensions with lower concentrations were generated by dilution with ultra pure water (Merck Millipore). To facilitate a uniform dispersion of the nanosilica, all solutions were stirred for 30 min by a magnetic stirrer prior to their use (either in spray printing setup or for suspension characterisation).

2.2.2. Suspension Rheology

For droplet generation, information on the rheological properties—especially at high solids loadings—is required. Previous studies on Drop-on-Demand Printing have shown that a dynamic viscosity of the suspension in the range of 1 to 50 mPa s is preferable for fast and reproducible droplet generation [23].

Characterisation of the dynamic viscosity was performed in a rheometer (MCR 302, Anton Paar GmbH, Ostfildern, Germany) using the coaxial cylinder geometry (DG26.7). The shear rate (at different concentrations) was varied in the range from 0.01 to 1000 s⁻¹ (at a constant temperature of 25 °C) to account for different stresses during the droplet generation, e.g., at the tip of the syringe. Furthermore, the viscosity dependence on the suspension temperature was studied in the range from 25 to 40 °C (at a fixed shear rate of 1000 s⁻¹).

For the range of shear rates specified, an almost constant viscosity of 1.5 mPa s was measured. Changing the temperature from 25 to 40 °C yielded a reduction in viscosity, which can be fully attributed to the decrease in viscosity of the base liquid (water): $\eta = 1.6$ mPa s at 25 °C to $\eta = 1.2$ mPa s at 40 °C.

2.2.3. Contact Angle and Surface Tension

Information on the contact angle and surface tension are required to design, e.g., the surface coverage of individual droplets on the substrate, and yield information on the limitations in local spatial resolution.

Determination of the (static) contact angle and surface tension of the nanosuspension were performed using an OCA 200 (DataPhysics Instruments GmbH, Germany). The contact angle on the glass substrate was measured using the sessile drop method; and determination of the surface tension was measured using the pendant drop method. For both setups, image acquisition and evaluation are performed by the integrated software (SCA, DataPhysics Instruments GmbH, Germany) based on evaluation of the Young(-Laplace) equation. Static contact angles were determined for droplets with a volume of 1.5 μL ; the surface tension measurements used larger droplets (droplet volume of 25 μL at a needle tip with diameter of 1.83 mm). The droplet volumes are adjusted for ease of evaluation by the software package.

For the suspension under consideration, a contact angle of 13.7° (cleaned but non-functionalised glass slide) and a surface tension of 86.7 mN/m were measured.

2.3. Characterisation of Porous Structure

Apart from the feasibility of the approach, packing porosity and pore size distribution of the structures are the key success indicators.

Non-destructive estimation of the average porosity of the generated porous structures was performed using the information of total mass m_{3D} and volume V_{3D} of the (intermediate) structure. Given this information and the skeletal mass density of silica, ρ_s the average porosity was obtained via

$$\bar{\epsilon} = 1 - \frac{\rho_{3D}}{\rho_s}, \quad (1)$$

where $\rho_{3D} = m_{3D}/V_{3D}$. The mass of the structure was obtained by weighing with a resolution of 0.1 mg (Sartorius AG, Göttingen, Germany, model 320G). The total volume of the structure was obtained from images (photographs or SEM images depending on structure dimensions).

Detailed textural characterisation of the porous structure was performed by advanced gas physisorption based on a combination of Ar 87 K and N₂ 77 K adsorption. All samples were degassed at 150 °C under vacuum prior to each measurement. All physisorption experiments were performed with an Autosorb IQ (QuantaTec, Anton Paar). Ar 87 K isotherms were measured over the whole pressure range (with the relative pressure p/p_0 ranging from approximately 10^{-5} up to 1). N₂ 77 K isotherms were determined in a relative pressure range from $p/p_0 = 10^{-2}$ up to 1. The pore network and connectivity were analysed by comparing the pore size distributions determined from the adsorption and desorption branches.

3. Results and Discussion

In this section, we present two examples to highlight the capabilities of the approach and discuss the general operational issues in spray printing and further steps to improve and enhance the properties of the generated porous structures.

In Figure 3, a rectangular packing generated by spray printing is shown. The dimensions are: length = 46 mm (left to right); width = 23 mm and a height of 1 mm. The packing comprises 60 layers, i.e., each layer contributes on average a height of 16.6 μm . With a total mass of 0.97 g and a total volume of 1.06 cm^3 , an average porosity of 0.59 is achieved. Due to its dimensions, we refer to it in the following as a "thin-layer" structure.

For further investigation of the pore space, the packing has been cut into 3 strips of equal width along its length. In the following, the subsamples are denoted by their original position, i.e., "left", "middle", and "right". Figure 4a shows the comparison of N₂ adsorption isotherms for the three subsamples. The perfect agreement of the N₂ 77 K physisorption isotherms for all three subsample signals have similar textural properties, as shown in Table 1. This highlights the capability of the approach to generate large-scale structures with consistent properties. Hence, we focus solely on the detailed textural characterization of the left subsample in Figure 4b–d.

The Ar 87 K and N₂ 77 K isotherms shown in Figure 4b are of type IV(a) [24], indicating that mesopores are present in the sample. Figure 4c shows excellent agreement of the pore size distributions determined from Ar 87 K and N₂ 77 K adsorption and from Ar 87 K and N₂ 77 K desorption, respectively.

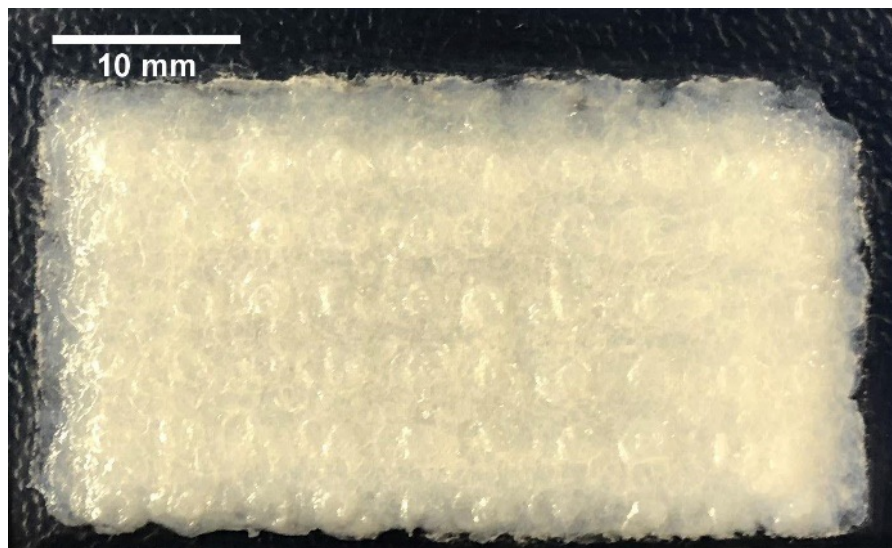


Figure 3. Exemplary result of a thin-layer packing. Dimensions: length = 46 mm (left to right); width = 23 mm, and a height 1 mm; average porosity 0.59.

From the adsorption branch in Figure 4d, it can be inferred that two major types of pores are formed: one type with pore sizes clustered around 10 nm, and the second type with larger pore sizes between 20 and 30 nm. The first type of pore is generated by the voids generated between contacting primary silica particles. The second type of pores with larger pore sizes are due to the structure formed during drying of the deposited droplet. Under the drying conditions used in the study, a torus-like solids pattern develops from the sessile droplet. The measured large pore diameters correspond to the central void (“hole”) of the torus. Overlapping of these voids by the solid material of later layers may partially restrict access to these pores. The extent of this and also opportunities to manipulate the occurrences and extent of larger pores, e.g., by droplet deposition pattern and drying conditions, is currently under investigation.

The detailed discussion of the measured pore size distribution is divided into two parts in the following: first, for pores smaller than 15 nm; and second, for pores larger than 15 nm. For pores smaller than 15 nm, we find a small shift of the pore size distribution determined from the adsorption branch to smaller pore sizes compared to the pore size distribution from the desorption branch. This observation can be attributed to initiated/advanced condensation, i.e., the effective nucleation barrier associated with the nucleation of the liquid phase is reduced in an interconnected pore network, resulting in a phase transition at a relative pressure smaller than the relative pressure associated with the spinodal of the fluid in these pores [25–27]. The occurrence of the initiated condensation is known to occur in highly connected 3D pore networks [25]. For these pores, the desorption branch reflects thermodynamic equilibrium and the pore size can be determined in a straightforward way from the desorption branch.

However, for pores larger than 15 nm, a shift of the pore size distribution determined from the desorption branch to smaller pore sizes can be observed, which is caused by pore blocking. Hence, some of the larger mesopores are restricted by smaller pore necks and these pores remain filled until the necks evaporate at a lower relative pressure during the desorption process. For these pores, the pore size distribution can be reliably determined from the adsorption branch of the N₂ 77 K and Ar 87 K isotherms, respectively.

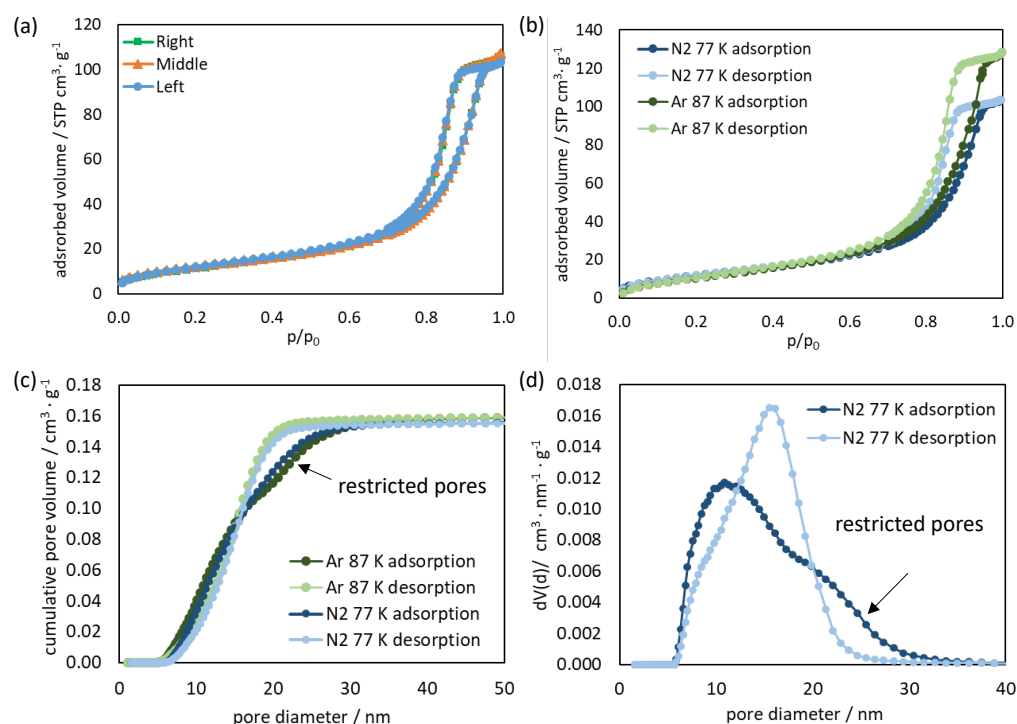


Figure 4. Textural characterization of thin-layer packing. (a) N_2 77 K adsorption isotherms of the three subsamples (left, middle and right part), (b) N_2 77 K and Ar 87 K adsorption isotherms of the left sample, (c) cumulative pore volume determined from the Ar 87 K and N_2 77 K adsorption branches using a dedicated NLDFT metastable adsorption branch kernel (assuming N_2 and Ar adsorption, respectively in cylindrical silica pores) in comparison with the cumulative pore volume determined from the Ar 87 K and N_2 77 K desorption branches using the corresponding NLDFT equilibrium kernel and (d) pore size distribution calculated from the N_2 77 K adsorption branch using a dedicated NLDFT metastable adsorption kernel and from the N_2 desorption branch using a dedicated NLDFT equilibrium kernel.

Table 1 summarizes the textural properties of the three subsamples. The pore volume determined via the Gurvich rule at a relative pressure $p/p_0 = 0.98$ is essentially the same as the pore volume determined with NLDFT (see Figure 4c). The specific surface area of the subsamples was evaluated using the BET method based on Ar 87 K adsorption, as the choice of N_2 as a probe molecule for surface area assessment can lead to an overestimation of the specific surface area of approx. 20% [28].

Table 1. Textural properties of the three subsamples (left, middle, right) of the thin-layer porous structure. The surface areas determined by the BET method based on Ar 87 K adsorption for a relative pressure range from $p/p_0 = 0.05$ – 0.3 . Pore volume (N_2 77 K and Ar 87 K) was determined using the Gurvich equation at $p/p_0 = 0.98$ with NLDFT.

Subsample	Surface Area (Ar 87 K)/ $m^2 g^{-1}$	Pore Volume (Ar 87 K)/ $cm^3 g^{-1}$	Pore Volume (N_2 77 K)/ $cm^3 g^{-1}$
Left	38.7	0.16	0.16
Middle	38.4	0.16	0.16
Right	35.7	0.16	0.16

Finally, we note that packings of this size may already be relevant for chromatographic applications, i.e., the presented technique is of practical use.

Moreover, pillar-like structures that resemble chromatographic packings can be generated directly by this approach. Figure 5 presents a current outcome. The trapezoidal packing has the following dimensions: a quadratic base with a side-length of 11 mm and a height of 13 mm; it comprises 225 layers in total.

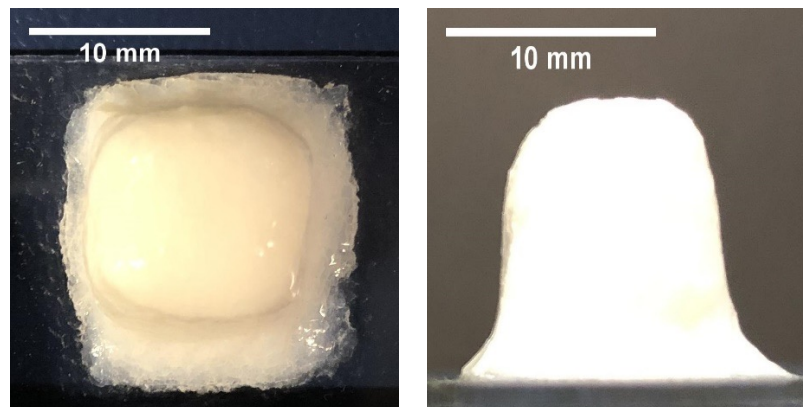


Figure 5. Exemplary result of a spray-printed pillar-like structure (dimensions: 11 mm by 11 mm by 13 mm; 225 layers). Left: top-view. Right: side-view.

With a total mass of 2.65 g, the average porosity yields 0.24, i.e., it is significantly denser than the thin-layer structure. This may be due to additional pressure on each layer due to the mass of material placed on top of it. This densification may be overcome by adding inert spacer materials, e.g., [14], where waxes were used that were washed out from the generated structure. Another aspect that requires improvement is the dimensional accuracy, especially towards the top of the structure. Effects observed at the bottom can be manipulated by changing the contact angle of the suspension with the substrate such that the droplets do not spread as widely. This and the smoothing effect at the edges can be suppressed by simultaneously manufacturing suitable support structures, e.g., by one of the other syringes. Here, new and exciting opportunities for packing and structure design are opened.

Apart from these observations, general operational challenges exist that are addressed in the following.

3.1. Operational Challenges and Counter-Measures

Here, we report common challenges in the spray printing of porous substrates that may lead to breakdown of operation, minor and major defects in the spray printed structures. We also discuss strategies by which those challenges can be overcome or their occurrence be minimised.

The main challenges are summarised in Figure 6. Note that several of the issues may appear simultaneously, depending on the operation parameters. Failure of the production process is highly likely if at least one of the challenges is present.

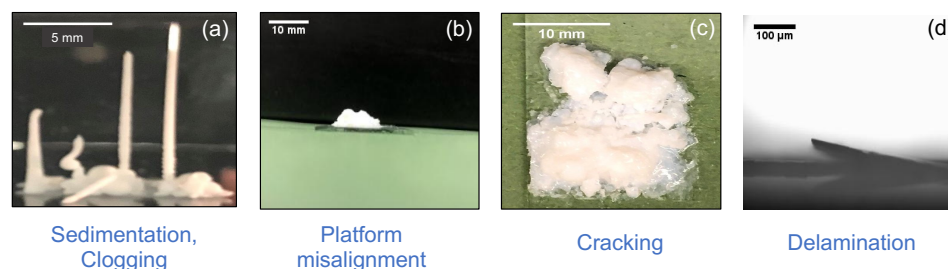


Figure 6. Typical challenges in spray printing of nanosuspensions. Failure of substrate construction is likely, even if only one of these effects occur.

3.1.1. Syringe Clogging

A major problem of the spray printing setup is clogging of the syringe due to drying of the suspension at the syringe tip. The needle of the syringe is exposed to the heated gas, which is transferred through the material to the suspension. Due to this heat transfer, liquid evaporates. Combined with the drying time of the layer of deposited droplets during which the syringe is not operating, enough liquid can evaporate from the needle such that a solid packing is formed in the needle, preventing further droplet dispensing. The smaller the needle diameter, the smaller the liquid volume and the faster clogging occurs. In order to continue spray printing, the needle needs to be cleaned manually, reducing the productivity of the setup.

This challenge can be solved in at least three ways: the use of needles with larger diameters (only possible, if the generated droplets are still in the acceptable range); thermal insulation of the needle (jacketing) to limit heat transfer from the gas to the needle; and designing dispensing paths such that resting times for drying are minimised and continuous dispensing of droplets is achieved.

3.1.2. Spacing Effect

The correct and uniform positioning of droplets onto the glass substrate or the top layer of deposits does not allow for arbitrary spacings Δz between the tip of the needle and the uppermost layer (or substrate). Different outcomes are exemplified in Figure 7.

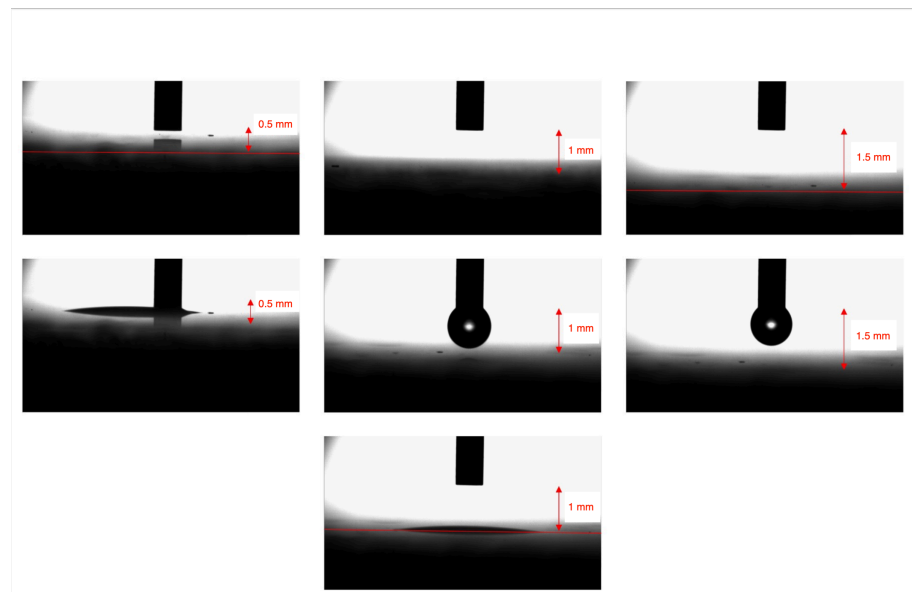


Figure 7. Droplet deposition outcomes for different syringe-platform spacings. Left column: spacing too low. Middle column: spacing too large, dispensing velocity too large (splashing or rebound of droplet upon contact with substrate). Right column: spacing too large and dispensing velocity too small (no detachment).

If Δz is too small compared to the intended droplet size (left column), the droplet is deformed upon deposition, leading to a larger footprint than intended. Depending on the interaction with the substrate or the porous layer, this footprint is kept throughout the drying process (“pinning”) yielding an unfavourable spatial distribution of nanoparticles.

If Δz is too large, the droplet is in free-fall upon dispensing. Depending on the dispensing velocity, the droplet will splash upon contact with the substrate (either material), generating satellite droplets of varying size (middle column). This also leads to an unfavourable distribution of the solids, reducing the achievable quality of the porous structure. If the dispensing velocity is too low, then the droplet may not detach from the needle tip (right column), i.e., no droplet is generated, leading to a (unintentional) non-uniform droplet pattern on the substrate.

From our trials, the optimum distance is such that the fully formed droplet is barely in contact with the previous layer or substrate. Upon release from the needle, it quickly relaxes into its equilibrium shape (spherical cap), dries and generates the intended solids deposition pattern. Given that the droplet volume is related to the droplet footprint, this distance can be calculated without problems, see, e.g., Rieck et al. [29].

3.1.3. Delamination

Separation of porous layers (delamination) during spray printing is occasionally observed. The main reasons are a lack of adhesion between layers due to weak interaction of the nanoparticles. Initially, adhesion is stronger due to the presence of liquid bridges between nanoparticles of different layers; with drying, this effect weakens. Droplet interaction with the top layer may also cause delamination, if the retraction force of the syringe is transferred directly to the top layer and overcomes the interaction forces between the (partially) dried nanoparticles.

Figure 6 shows a typical scenario where delamination occurs after a few layers. Neglecting the occurrence and subsequent build-up of additional layers yields unstable structures. The adhesion of further layers is locally weaker, which may lead to cracking of the structure. Empirically, it was observed that delamination preferentially starts near the corners and edges of the structures. This is to be expected as at those locations only partial interaction of the nanoparticles with each other can be realised due to the interface with the surrounding gas phase.

Delamination can be minimised by either strengthening the interaction between individual nanoparticles (by suitable functionalisation), slow retraction of the syringe after droplet position, optimisation of the drying conditions to prevent thermal stress during organisation and adhesion of the nanoparticles, and the supply of encompassing support structures during preparation of the spray printed substrate.

4. Conclusions and Outlook

In this work, we presented a technology that allows the continuous production of porous substrates from nanosuspensions by spray printing, i.e., the layer-by-layer build-up of the substrate from single droplets. The droplets are dried by a convective gas flow, and the remaining solid deposits form the porous structure.

The main results and conclusions are:

- Using spray printing porous substrates relevant for chromatography can be produced from nanosuspensions by convective drying.
- Using colloidal silica (45 nm) in water, consistent porosity and pore size distribution can be achieved along the substrate (packing).
- In the system under consideration, the pore sizes fall into two categories, <15 nm and >15 nm, i.e., there exists the opportunity to fine-tune pore size during manufacturing.
- Several operational challenges exist that can be overcome by suitable tuning of nanosuspension rheology and process conditions, especially drying conditions.
- Some problems with dimensional accuracy still persists, but can be solved, e.g., by simultaneous construction of support structures that are removed afterwards.

Future work is concerned with the generation of defined gradients in the properties of the structure, e.g., by manipulation of the type of particles in the suspension (size, concentration), the temporary embedding of spacer particles, or the drying conditions.

Author Contributions: Conceptualization, D.H.P.V. and A.B.; methodology, D.H.P.V. and A.B.; software, formal analysis, A.B.; investigation, D.H.P.V. and C.S.; writing—original draft preparation, D.H.P.V. and C.S.; writing—review and editing, D.H.P.V., C.S. and A.B.; supervision, A.B.; project administration, M.T. and A.B.; funding acquisition, M.T. and A.B. All authors have read and agreed to the published version of the manuscript.

Funding: This research was funded by German Research Foundation (DFG) within the collaborative research center 1411 “Design of Particulate Products”—Project ID 416229255 (projects B02, B03). We acknowledge financial support from German Research Foundation and Friedrich-Alexander-Universität Erlangen-Nürnberg within the funding program “Open Access Publication Funding”.

Institutional Review Board Statement: Not applicable

Informed Consent Statement: Not applicable

Data Availability Statement: Data are available from the corresponding author upon reasonable request.

Conflicts of Interest: The authors declare no conflict of interest. The funders had no role in the design of the study; in the collection, analyses, or interpretation of data; in the writing of the manuscript; or in the decision to publish the results.

Abbreviations

The following abbreviations are used in this manuscript:

NLDFT	Nonlocal density functional theory
SPM	Stationary phase material

References

1. Walton, D.; Mumford, C. The Morphology of Spray-Dried Particles: The Effect of Process Variables upon the Morphology of Spray-Dried Particles. *Chem. Eng. Res. Des.* **1999**, *77*, 442–460. [\[CrossRef\]](#)
2. Martin, H. Low-Peclet number particle-to-fluid heat and mass transfer in packed beds. *Chem. Eng. Sci.* **1978**, *33*, 913–919. [\[CrossRef\]](#)
3. Op De Beeck, J.; Callewaert, M.; Ottevaere, H.; Gardeniers, H.; Desmet, G.; Malsche, W.D. On the advantages of radially elongated structures in microchip-based liquid chromatography. *Anal. Chem.* **2013**, *85*, 5207–5213. [\[CrossRef\]](#) [\[PubMed\]](#)
4. Arrua, R.; Causon, T.; Hilder, E. Recent developments and future possibilities for polymer monoliths in separation science. *Analyst* **2012**, *137*, 5169–5178. [\[CrossRef\]](#) [\[PubMed\]](#)
5. Berneman, N.; Jimidar, I.; Geite, W.V.; Gardeniers, H.; Desmet, G. Rapid vacuum driven monolayer assembly of microparticles on the surface of perforated microfluidic devices. *Powder Technol.* **2021**, *390*, 330–338. [\[CrossRef\]](#)
6. Van Geite, W.; Jimidar, I.; Sotthewes, K.; Gardeniers, H.; Desmet, G. Vacuum-driven assembly of electrostatically levitated microspheres on perforated surfaces. *Mater. Des.* **2021**, *216*, 110573. [\[CrossRef\]](#)
7. Inayat, A.; Schwerdtfeger, J.; Freund, H.; Körner, C.; Singer, R.F.; Schwieger, W. Periodic open-cellfoams: Pressure drop measurements and modeling of an ideal tetrakaidecahedra packing. *Chem. Eng. Sci.* **2011**, *66*, 2758–2763. [\[CrossRef\]](#)
8. Sandron, S.; Heery, B.; Gupta, V.; Collins, D.; Nesterenko, E.; Nesterenko, P.; Talebi, M.; Beirne, S.; Thompson, F.; Wall, G. 3D printed metal columns for capillary liquid chromatography. *Analyst* **2014**, *139*, 6343–6347. [\[CrossRef\]](#)
9. Kolaczowska, S.; Awdrya, S.; Smith, T.; Thomas, D.; Torkuhl, L.; Kolvenbach, R. Potential for metal foams to act as structured catalyst supports infixed-bed reactors. *Catal. Today* **2016**, *273*, 221–233. [\[CrossRef\]](#)
10. Arita, R.; Iijima, M.; Fujishiro, Y.; Morita, S.; Furukawa, T.; Tatami, J.; Maruo, S. Rapid three-dimensional structuring of transparent SiO₂ glass using interparticle photo-cross-linkable suspensions. *Nat. Commun. Mater.* **2020**, *1*, 30. [\[CrossRef\]](#)
11. Komori, T.; Furukawa, T.; Iijima, M.; Maruo, S. Multi-scale laser direct writing of conductive metal microstructures using a 405-nm blue laser. *Opt. Express* **2020**, *28*, 8363–8370. [\[CrossRef\]](#)
12. Morita, S.; Iijima, M.; Chen, Y.; Furukawa, T.; Tatami, J.; Maruo, S. 3D structuring of dense alumina ceramics using fiber-based stereolithography with interparticle photo-cross-linkable slurry. *Adv. Powder Technol.* **2021**, *32*, 72–79. [\[CrossRef\]](#)
13. Juodkazis, S.; Mizeikis, V.; Seet, K.K.; Miwa, M.; Misawa, H. Two-photon lithography of nanorods in SU-8 photoresist. *Nanotechnology* **2005**, *16*, 846–849. [\[CrossRef\]](#)
14. Dimartino, S.; Galindo-Rodriguez, G.; Simon, U.; Conti, M.; Sarwar, M.S.; Narayanan, S.A.; Jiang, Q.; Christofi, N. Flexible material formulations for 3D printing of ordered porous beds with applications in bioprocess engineering. *Bioresour. Bioprocess.* **2022**, *9*, 20. [\[CrossRef\]](#)
15. Nawada, S.; Dimartino, S.; Fee, C. Dispersion behavior of 3D-printed columns with homogeneous microstructures comprising differing element shapes. *Chem. Eng. Sci.* **2017**, *164*, 90–98. [\[CrossRef\]](#)
16. Deegan, R.; Bakajin, O.; Dupont, T.; Huber, G.; Nagel, S.; Witten, T. Capillary flow as the cause of ring stains from dried liquid droplets. *Nature* **1997**, *389*, 827–829. [\[CrossRef\]](#)
17. Larson, R. Transport and deposition patterns in drying sessile droplets Transport and deposition patterns in drying sessile droplets. *AIChE J.* **2014**, *60*, 1538–1571. [\[CrossRef\]](#)
18. Sondej, F.; Peglow, M.; Bück, A.; Tsotsas, E. Experimental investigation of the morphology of salt deposits from drying sessile droplets by white-light interferometry. *AIChE J.* **2018**, *64*, 2002–2016. [\[CrossRef\]](#)

19. Style, R.; Peppin, S. Crust formation in drying colloidal suspensions. *Proc. R. Soc. A Math. Phys. Eng. Sci.* **2010**, *467*, 174–193. [[CrossRef](#)]
20. Schweitzer, J.M.; Servel, M.; Salvatori, F.; Dandeu, A.; Minière, M.; Joly, J.F.; Gaubert, Q.; Barbosa, S.; Onofri, F. Spray drying of colloidal suspensions: Coupling of particle drying and transport models with experimental validations. *Chem. Eng. Res. Des.* **2021**, *170*, 224–238. [[CrossRef](#)]
21. Janocha, M.; Tsotsas, E. In silico investigation of the evaporation flux distribution along sessile droplet surfaces during convective drying. *Chem. Eng. Sci.* **2021**, *238*, 116590. [[CrossRef](#)]
22. Janocha, M.; Tsotsas, E. Coating layer formation from deposited droplets—A comparison of nanofluid, microfluid and solution. *Powder Technol.* **2022**, *399*, 117202. [[CrossRef](#)]
23. Hutchings, I.; Martin, G. *Inkjet Technology for Digital Fabrication*; Wiley: Hoboken, NJ, USA, 2012.
24. Thommes, M.; Kaneko, K.; Neimark, A.; Olivier, J.; Rodriguez-Reinoso, F.; Rouquerol, J.; Sing, K. Physisorption of Gases, with Special Reference to the Evaluation of Surface Area and Pore Size Distribution (IUPAC Technical Report). *Pure Appl. Chem.* **2015**, *87*, 1051–1069. [[CrossRef](#)]
25. Kleitz, F.; Bérubé, F.; Guillet-Nicolas, R.; Yang, C.M.; Thommes, M. Probing Adsorption, Pore Condensation, and Hysteresis Behavior of Pure Fluids in Three-Dimensional Cubic Mesoporous KIT-6 Silica. *J. Phys. Chem. C* **2010**, *114*, 9344–9355. [[CrossRef](#)]
26. Guillet-Nicolas, R.; Bérubé, F.; Thommes, M.; Janicke, M.; Kleitz, F. Selectively Tuned Pore Condensation and Hysteresis Behavior in Mesoporous SBA-15 Silica: Correlating Material Synthesis to Advanced Gas Adsorption Analysis. *J. Phys. Chem. C* **2017**, *121*, 24505–24526. [[CrossRef](#)]
27. Schlumberger, C.; Thommes, M. Characterization of Hierarchically Ordered Porous Materials by Physisorption and Mercury Porosimetry—A Tutorial Review. *Adv. Mater. Interfaces* **2021**, *8*, 2002181. [[CrossRef](#)]
28. Schlumberger, C.; Scherdel, C.; Kriesten, M.; Leicht, P.; Keilbach, H.E.A.; Kotnik, P.; Reichenauer, G.; Thommes, M. Reliable Surface Area Determination of Powders and Meso/Macroporous Materials: Small-Angle X-Ray Scattering and Gas Physisorption. *Microporous Mesoporous Mater.* **2022**, *329*, 111554. [[CrossRef](#)]
29. Rieck, C.; Bück, A.; Tsotsas, E. Estimation of the dominant size enlargement mechanism in spray fluidized bed processes. *AIChE J.* **2020**, *66*, e16929. [[CrossRef](#)]

Disclaimer/Publisher’s Note: The statements, opinions and data contained in all publications are solely those of the individual author(s) and contributor(s) and not of MDPI and/or the editor(s). MDPI and/or the editor(s) disclaim responsibility for any injury to people or property resulting from any ideas, methods, instructions or products referred to in the content.